

# Measurement of the Mass and Width and Study of the Spin of the $\Xi(1690)^0$ Resonance from $\Lambda_c^+ \rightarrow \Lambda \bar{K}^0 K^+$ Decay at *BABAR*

The *BABAR* Collaboration

October 3, 2018

## Abstract

The  $\Xi(1690)^0$  resonance is observed in the  $\Lambda \bar{K}^0$  channel in the decay  $\Lambda_c^+ \rightarrow \Lambda \bar{K}^0 K^+$ , from a data sample corresponding to a total integrated luminosity of  $\sim 200 \text{ fb}^{-1}$  recorded by the *BABAR* detector at the PEP-II asymmetric-energy  $e^+e^-$  collider operating at  $\sim 10.58 \text{ GeV}$  and  $\sim 10.54 \text{ GeV}$  center-of-mass energies. A fit to the Dalitz plot intensity distribution corresponding to the coherent superposition of amplitudes describing  $\Lambda a_0(980)^+$  and  $\Xi(1690)^0 K^+$  production yields mass and width values of  $1684.7 \pm 1.3$  (stat.)  $_{-1.6}^{+2.2}$  (syst.)  $\text{ MeV}/c^2$ , and  $8.1_{-3.5}^{+3.9}$  (stat.)  $_{-0.9}^{+1.0}$  (syst.)  $\text{ MeV}$ , respectively, for the  $\Xi(1690)^0$ , while the spin is found to be consistent with value of  $1/2$  on the basis of studies of the  $(\Lambda K_S)$  angular distribution.

Submitted to the 33<sup>rd</sup> International Conference on High-Energy Physics, ICHEP 06,  
26 July—2 August 2006, Moscow, Russia.

*Stanford Linear Accelerator Center, Stanford University, Stanford, CA 94309*

---

Work supported in part by Department of Energy contract DE-AC03-76SF00515.

The BABAR Collaboration,

B. Aubert, R. Barate, M. Bona, D. Boutigny, F. Couderc, Y. Karyotakis, J. P. Lees, V. Poireau,  
V. Tisserand, A. Zghiche

*Laboratoire de Physique des Particules, IN2P3/CNRS et Université de Savoie, F-74941 Annecy-Le-Vieux,  
France*

E. Grauges

*Universitat de Barcelona, Facultat de Física, Departament ECM, E-08028 Barcelona, Spain*

A. Palano

*Università di Bari, Dipartimento di Fisica and INFN, I-70126 Bari, Italy*

J. C. Chen, N. D. Qi, G. Rong, P. Wang, Y. S. Zhu

*Institute of High Energy Physics, Beijing 100039, China*

G. Eigen, I. Ofte, B. Stugu

*University of Bergen, Institute of Physics, N-5007 Bergen, Norway*

G. S. Abrams, M. Battaglia, D. N. Brown, J. Button-Shafer, R. N. Cahn, E. Charles, M. S. Gill,  
Y. Groyzman, R. G. Jacobsen, J. A. Kadyk, L. T. Kerth, Yu. G. Kolomensky, G. Kukartsev, G. Lynch,  
L. M. Mir, T. J. Orimoto, M. Pripstein, N. A. Roe, M. T. Ronan, W. A. Wenzel

*Lawrence Berkeley National Laboratory and University of California, Berkeley, California 94720, USA*

P. del Amo Sanchez, M. Barrett, K. E. Ford, A. J. Hart, T. J. Harrison, C. M. Hawkes, S. E. Morgan,  
A. T. Watson

*University of Birmingham, Birmingham, B15 2TT, United Kingdom*

T. Held, H. Koch, B. Lewandowski, M. Pelizaeus, K. Peters, T. Schroeder, M. Steinke  
*Ruhr Universität Bochum, Institut für Experimentalphysik 1, D-44780 Bochum, Germany*

J. T. Boyd, J. P. Burke, W. N. Cottingham, D. Walker

*University of Bristol, Bristol BS8 1TL, United Kingdom*

D. J. Asgeirsson, T. Cuhadar-Donszelmann, B. G. Fulsom, C. Hearty, N. S. Knecht, T. S. Mattison,  
J. A. McKenna

*University of British Columbia, Vancouver, British Columbia, Canada V6T 1Z1*

A. Khan, P. Kyberd, M. Saleem, D. J. Sherwood, L. Teodorescu

*Brunel University, Uxbridge, Middlesex UB8 3PH, United Kingdom*

V. E. Blinov, A. D. Bukin, V. P. Druzhinin, V. B. Golubev, A. P. Onuchin, S. I. Serednyakov,  
Yu. I. Skovpen, E. P. Solodov, K. Yu Todyshev

*Budker Institute of Nuclear Physics, Novosibirsk 630090, Russia*

D. S. Best, M. Bondioli, M. Bruinsma, M. Chao, S. Curry, I. Eschrich, D. Kirkby, A. J. Lankford, P. Lund,  
M. Mandelkern, R. K. Mommsen, W. Roethel, D. P. Stoker

*University of California at Irvine, Irvine, California 92697, USA*

S. Abachi, C. Buchanan

*University of California at Los Angeles, Los Angeles, California 90024, USA*

S. D. Foulkes, J. W. Gary, O. Long, B. C. Shen, K. Wang, L. Zhang  
*University of California at Riverside, Riverside, California 92521, USA*

H. K. Hadavand, E. J. Hill, H. P. Paar, S. Rahatlou, V. Sharma  
*University of California at San Diego, La Jolla, California 92093, USA*

J. W. Berryhill, C. Campagnari, A. Cunha, B. Dahmes, T. M. Hong, D. Kovalskyi, J. D. Richman  
*University of California at Santa Barbara, Santa Barbara, California 93106, USA*

T. W. Beck, A. M. Eisner, C. J. Flacco, C. A. Heusch, J. Kroseberg, W. S. Lockman, G. Nesom, T. Schalk,  
B. A. Schumm, A. Seiden, P. Spradlin, D. C. Williams, M. G. Wilson  
*University of California at Santa Cruz, Institute for Particle Physics, Santa Cruz, California 95064, USA*

J. Albert, E. Chen, A. Dvoretzkii, F. Fang, D. G. Hitlin, I. Narsky, T. Piatenko, F. C. Porter, A. Ryd,  
A. Samuel  
*California Institute of Technology, Pasadena, California 91125, USA*

G. Mancinelli, B. T. Meadows, K. Mishra, M. D. Sokoloff  
*University of Cincinnati, Cincinnati, Ohio 45221, USA*

F. Blanc, P. C. Bloom, S. Chen, W. T. Ford, J. F. Hirschauer, A. Kreisel, M. Nagel, U. Nauenberg,  
A. Olivas, W. O. Ruddick, J. G. Smith, K. A. Ulmer, S. R. Wagner, J. Zhang  
*University of Colorado, Boulder, Colorado 80309, USA*

A. Chen, E. A. Eckhart, A. Soffer, W. H. Toki, R. J. Wilson, F. Winklmeier, Q. Zeng  
*Colorado State University, Fort Collins, Colorado 80523, USA*

D. D. Altenburg, E. Feltresi, A. Hauke, H. Jasper, J. Merkel, A. Petzold, B. Spaan  
*Universität Dortmund, Institut für Physik, D-44221 Dortmund, Germany*

T. Brandt, V. Klose, H. M. Lacker, W. F. Mader, R. Nogowski, J. Schubert, K. R. Schubert, R. Schwierz,  
J. E. Sundermann, A. Volk  
*Technische Universität Dresden, Institut für Kern- und Teilchenphysik, D-01062 Dresden, Germany*

D. Bernard, G. R. Bonneaud, E. Latour, Ch. Thiebaux, M. Verderi  
*Laboratoire Leprince-Ringuet, CNRS/IN2P3, Ecole Polytechnique, F-91128 Palaiseau, France*

P. J. Clark, W. Gradl, F. Muheim, S. Playfer, A. I. Robertson, Y. Xie  
*University of Edinburgh, Edinburgh EH9 3JZ, United Kingdom*

M. Andreotti, D. Bettoni, C. Bozzi, R. Calabrese, G. Cibinetto, E. Luppi, M. Negrini, A. Petrella,  
L. Piemontese, E. Prencipe  
*Università di Ferrara, Dipartimento di Fisica and INFN, I-44100 Ferrara, Italy*

F. Anulli, R. Baldini-Ferroli, A. Calcaterra, R. de Sangro, G. Finocchiaro, S. Pacetti, P. Patteri,  
I. M. Peruzzi,<sup>1</sup> M. Piccolo, M. Rama, A. Zallo  
*Laboratori Nazionali di Frascati dell'INFN, I-00044 Frascati, Italy*

---

<sup>1</sup>Also with Università di Perugia, Dipartimento di Fisica, Perugia, Italy

A. Buzzo, R. Capra, R. Contri, M. Lo Vetere, M. M. Macri, M. R. Monge, S. Passaggio, C. Patrignani,  
E. Robutti, A. Santroni, S. Tosi

*Università di Genova, Dipartimento di Fisica and INFN, I-16146 Genova, Italy*

G. Brandenburg, K. S. Chaisanguanthum, M. Morii, J. Wu

*Harvard University, Cambridge, Massachusetts 02138, USA*

R. S. Dubitzky, J. Marks, S. Schenk, U. Uwer

*Universität Heidelberg, Physikalisches Institut, Philosophenweg 12, D-69120 Heidelberg, Germany*

D. Bard, W. Bhimji, D. A. Bowerman, P. D. Dauncey, U. Egede, R. L. Flack, J. A. Nash, M. B. Nikolich,  
W. Panduro Vazquez

*Imperial College London, London, SW7 2AZ, United Kingdom*

P. K. Behera, X. Chai, M. J. Charles, U. Mallik, N. T. Meyer, V. Ziegler

*University of Iowa, Iowa City, Iowa 52242, USA*

J. Cochran, H. B. Crawley, L. Dong, V. Eyges, W. T. Meyer, S. Prell, E. I. Rosenberg, A. E. Rubin

*Iowa State University, Ames, Iowa 50011-3160, USA*

A. V. Gritsan

*Johns Hopkins University, Baltimore, Maryland 21218, USA*

A. G. Denig, M. Fritsch, G. Schott

*Universität Karlsruhe, Institut für Experimentelle Kernphysik, D-76021 Karlsruhe, Germany*

N. Arnaud, M. Davier, G. Grosdidier, A. Höcker, F. Le Diberder, V. Lepeltier, A. M. Lutz, A. Oyanguren,  
S. Pruvot, S. Rodier, P. Roudeau, M. H. Schune, A. Stocchi, W. F. Wang, G. Wormser

*Laboratoire de l'Accélérateur Linéaire, IN2P3/CNRS et Université Paris-Sud 11, Centre Scientifique  
d'Orsay, B.P. 34, F-91898 ORSAY Cedex, France*

C. H. Cheng, D. J. Lange, D. M. Wright

*Lawrence Livermore National Laboratory, Livermore, California 94550, USA*

C. A. Chavez, I. J. Forster, J. R. Fry, E. Gabathuler, R. Gamet, K. A. George, D. E. Hutchcroft,  
D. J. Payne, K. C. Schofield, C. Touramanis

*University of Liverpool, Liverpool L69 7ZE, United Kingdom*

A. J. Bevan, F. Di Lodovico, W. Menges, R. Sacco

*Queen Mary, University of London, E1 4NS, United Kingdom*

G. Cowan, H. U. Flaecher, D. A. Hopkins, P. S. Jackson, T. R. McMahon, S. Ricciardi, F. Salvatore,  
A. C. Wren

*University of London, Royal Holloway and Bedford New College, Egham, Surrey TW20 0EX, United  
Kingdom*

D. N. Brown, C. L. Davis

*University of Louisville, Louisville, Kentucky 40292, USA*

J. Allison, N. R. Barlow, R. J. Barlow, Y. M. Chia, C. L. Edgar, G. D. Lafferty, M. T. Naisbit,  
J. C. Williams, J. I. Yi

*University of Manchester, Manchester M13 9PL, United Kingdom*

C. Chen, W. D. Hulsbergen, A. Jawahery, C. K. Lae, D. A. Roberts, G. Simi

*University of Maryland, College Park, Maryland 20742, USA*

G. Blaylock, C. Dallapiccola, S. S. Hertzbach, X. Li, T. B. Moore, S. Saremi, H. Staengle

*University of Massachusetts, Amherst, Massachusetts 01003, USA*

R. Cowan, G. Sciolla, S. J. Sekula, M. Spitznagel, F. Taylor, R. K. Yamamoto

*Massachusetts Institute of Technology, Laboratory for Nuclear Science, Cambridge, Massachusetts 02139,  
USA*

H. Kim, S. E. McLachlin, P. M. Patel, S. H. Robertson

*McGill University, Montréal, Québec, Canada H3A 2T8*

A. Lazzaro, V. Lombardo, F. Palombo

*Università di Milano, Dipartimento di Fisica and INFN, I-20133 Milano, Italy*

J. M. Bauer, L. Cremaldi, V. Eschenburg, R. Godang, R. Kroeger, D. A. Sanders, D. J. Summers,  
H. W. Zhao

*University of Mississippi, University, Mississippi 38677, USA*

S. Brunet, D. Côté, M. Simard, P. Taras, F. B. Viaud

*Université de Montréal, Physique des Particules, Montréal, Québec, Canada H3C 3J7*

H. Nicholson

*Mount Holyoke College, South Hadley, Massachusetts 01075, USA*

N. Cavallo,<sup>2</sup> G. De Nardo, F. Fabozzi,<sup>3</sup> C. Gatto, L. Lista, D. Monorchio, P. Paolucci, D. Piccolo,  
C. Sciacca

*Università di Napoli Federico II, Dipartimento di Scienze Fisiche and INFN, I-80126, Napoli, Italy*

M. A. Baak, G. Raven, H. L. Snoek

*NIKHEF, National Institute for Nuclear Physics and High Energy Physics, NL-1009 DB Amsterdam, The  
Netherlands*

C. P. Jessop, J. M. LoSecco

*University of Notre Dame, Notre Dame, Indiana 46556, USA*

T. Allmendinger, G. Benelli, L. A. Corwin, K. K. Gan, K. Honscheid, D. Hufnagel, P. D. Jackson,  
H. Kagan, R. Kass, A. M. Rahimi, J. J. Regensburger, R. Ter-Antonyan, Q. K. Wong

*Ohio State University, Columbus, Ohio 43210, USA*

N. L. Blount, J. Brau, R. Frey, O. Igonkina, J. A. Kolb, M. Lu, R. Rahmat, N. B. Sinev, D. Strom,  
J. Strube, E. Torrence

*University of Oregon, Eugene, Oregon 97403, USA*

---

<sup>2</sup>Also with Università della Basilicata, Potenza, Italy

<sup>3</sup>Also with Università della Basilicata, Potenza, Italy

A. Gaz, M. Margoni, M. Morandin, A. Pompili, M. Posocco, M. Rotondo, F. Simonetto, R. Stroili, C. Voci  
*Università di Padova, Dipartimento di Fisica and INFN, I-35131 Padova, Italy*

M. Benayoun, H. Briand, J. Chauveau, P. David, L. Del Buono, Ch. de la Vaissière, O. Hamon,  
B. L. Hartfiel, M. J. J. John, Ph. Leruste, J. Malcès, J. Ocariz, L. Roos, G. Therin  
*Laboratoire de Physique Nucléaire et de Hautes Energies, IN2P3/CNRS, Université Pierre et Marie  
Curie-Paris6, Université Denis Diderot-Paris7, F-75252 Paris, France*

L. Gladney, J. Panetta  
*University of Pennsylvania, Philadelphia, Pennsylvania 19104, USA*

M. Biasini, R. Covarelli  
*Università di Perugia, Dipartimento di Fisica and INFN, I-06100 Perugia, Italy*

C. Angelini, G. Batignani, S. Bettarini, F. Bucci, G. Calderini, M. Carpinelli, R. Cenci, F. Forti,  
M. A. Giorgi, A. Lusiani, G. Marchiori, M. A. Mazur, M. Morganti, N. Neri, G. Rizzo, J. J. Walsh  
*Università di Pisa, Dipartimento di Fisica, Scuola Normale Superiore and INFN, I-56127 Pisa, Italy*

M. Haire, D. Judd, D. E. Wagoner  
*Prairie View A&M University, Prairie View, Texas 77446, USA*

J. Biesiada, N. Danielson, P. Elmer, Y. P. Lau, C. Lu, J. Olsen, A. J. S. Smith, A. V. Telnov  
*Princeton University, Princeton, New Jersey 08544, USA*

F. Bellini, G. Cavoto, A. D’Orazio, D. del Re, E. Di Marco, R. Faccini, F. Ferrarotto, F. Ferroni,  
M. Gaspero, L. Li Gioi, M. A. Mazzoni, S. Morganti, G. Piredda, F. Polci, F. Safai Tehrani, C. Voena  
*Università di Roma La Sapienza, Dipartimento di Fisica and INFN, I-00185 Roma, Italy*

M. Ebert, H. Schröder, R. Waldi  
*Universität Rostock, D-18051 Rostock, Germany*

T. Adye, N. De Groot, B. Franek, E. O. Olaiya, F. F. Wilson  
*Rutherford Appleton Laboratory, Chilton, Didcot, Oxon, OX11 0QX, United Kingdom*

R. Aleksan, S. Emery, A. Gaidot, S. F. Ganzhur, G. Hamel de Monchenault, W. Kozanecki, M. Legendre,  
G. Vasseur, Ch. Yèche, M. Zito  
*DSM/Daphnia, CEA/Saclay, F-91191 Gif-sur-Yvette, France*

X. R. Chen, H. Liu, W. Park, M. V. Purohit, J. R. Wilson  
*University of South Carolina, Columbia, South Carolina 29208, USA*

M. T. Allen, D. Aston, R. Bartoldus, P. Bechtle, N. Berger, R. Claus, J. P. Coleman, M. R. Convery,  
M. Cristinziani, J. C. Dingfelder, J. Dorfan, G. P. Dubois-Felsmann, D. Dujmic, W. Dunwoodie,  
R. C. Field, T. Glanzman, S. J. Gowdy, M. T. Graham, P. Grenier,<sup>4</sup> V. Halyo, C. Hast, T. Hryn’ova,  
W. R. Innes, M. H. Kelsey, P. Kim, D. W. G. S. Leith, S. Li, S. Luitz, V. Luth, H. L. Lynch,  
D. B. MacFarlane, H. Marsiske, R. Messner, D. R. Muller, C. P. O’Grady, V. E. Ozcan, A. Perazzo,  
M. Perl, T. Pulliam, B. N. Ratcliff, A. Roodman, A. A. Salnikov, R. H. Schindler, J. Schwiening,  
A. Snyder, J. Stelzer, D. Su, M. K. Sullivan, K. Suzuki, S. K. Swain, J. M. Thompson, J. Va’vra, N. van

---

<sup>4</sup>Also at Laboratoire de Physique Corpusculaire, Clermont-Ferrand, France

Bakel, M. Weaver, A. J. R. Weinstein, W. J. Wisniewski, M. Wittgen, D. H. Wright, A. K. Yarritu, K. Yi,  
C. C. Young

*Stanford Linear Accelerator Center, Stanford, California 94309, USA*

P. R. Burchat, A. J. Edwards, S. A. Majewski, B. A. Petersen, C. Roat, L. Wilden

*Stanford University, Stanford, California 94305-4060, USA*

S. Ahmed, M. S. Alam, R. Bula, J. A. Ernst, V. Jain, B. Pan, M. A. Saeed, F. R. Wappler, S. B. Zain

*State University of New York, Albany, New York 12222, USA*

W. Bugg, M. Krishnamurthy, S. M. Spanier

*University of Tennessee, Knoxville, Tennessee 37996, USA*

R. Eckmann, J. L. Ritchie, A. Satpathy, C. J. Schilling, R. F. Schwitters

*University of Texas at Austin, Austin, Texas 78712, USA*

J. M. Izen, X. C. Lou, S. Ye

*University of Texas at Dallas, Richardson, Texas 75083, USA*

F. Bianchi, F. Gallo, D. Gamba

*Università di Torino, Dipartimento di Fisica Sperimentale and INFN, I-10125 Torino, Italy*

M. Bomben, L. Bosisio, C. Cartaro, F. Cossutti, G. Della Ricca, S. Dittongo, L. Lanceri, L. Vitale

*Università di Trieste, Dipartimento di Fisica and INFN, I-34127 Trieste, Italy*

V. Azzolini, N. Lopez-March, F. Martinez-Vidal

*IFIC, Universitat de Valencia-CSIC, E-46071 Valencia, Spain*

Sw. Banerjee, B. Bhuyan, C. M. Brown, D. Fortin, K. Hamano, R. Kowalewski, I. M. Nugent, J. M. Roney,  
R. J. Sobie

*University of Victoria, Victoria, British Columbia, Canada V8W 3P6*

J. J. Back, P. F. Harrison, T. E. Latham, G. B. Mohanty, M. Pappagallo

*Department of Physics, University of Warwick, Coventry CV4 7AL, United Kingdom*

H. R. Band, X. Chen, B. Cheng, S. Dasu, M. Datta, K. T. Flood, J. J. Hollar, P. E. Kutter, B. Mellado,  
A. Mihalyi, Y. Pan, M. Pierini, R. Prepost, S. L. Wu, Z. Yu

*University of Wisconsin, Madison, Wisconsin 53706, USA*

H. Neal

*Yale University, New Haven, Connecticut 06511, USA*

# 1 INTRODUCTION

Although considerable advances have been made in baryon spectroscopy over the past decade, there has been very little improvement in our knowledge of hyperon resonances since 1988. In particular, little is known about cascade resonances. Aside from the  $\Xi(1530)$ , all  $\Xi$  resonances rate below four stars according to the PDG ranking criteria [1]. The  $\Xi(1690)$  has been observed in the  $\Lambda\bar{K}$ ,  $\Sigma\bar{K}$  and  $\Xi\pi$  final states with various degrees of certainty. However, its quantum numbers have not yet been measured.

The first evidence for the  $\Xi(1690)$  came from the observation of a threshold enhancement in the  $\Sigma^{+,0}K^-$  mass spectrum, produced in the reaction  $K^-p \rightarrow (\Sigma^{+,0}K^-)K\pi$  at 4.2 GeV/ $c$  in a bubble chamber experiment [2]. There were also indications of signals in the  $(\Lambda\bar{K}^0)$  and  $(\Lambda K^-)$  channels. Subsequently, the  $\Xi(1690)^-$  was observed in a hyperon beam experiment at CERN, in which an enhancement around 1700 MeV/ $c^2$  was seen in  $(\Lambda K^-)$  pairs diffractively produced by a 116 GeV/ $c$   $\Xi^-$  beam [3, 4]. The  $\Xi^-\pi^+$  decay mode of the  $\Xi(1690)^0$  was first reported by the WA89 Collaboration on the basis of a clear peak in the  $\Xi^-\pi^+$  mass spectrum resulting from the interactions of a 345 GeV/ $c$   $\Sigma^-$  beam in copper and carbon targets [5]. Evidence of  $\Xi(1690)^0$  production in  $\Lambda_c^+$  decay was reported by the Belle experiment, on the basis of  $246 \pm 20$   $\Lambda_c^+ \rightarrow (\Sigma^+K^-)K^+$  and  $363 \pm 26$   $\Lambda_c^+ \rightarrow (\Lambda\bar{K}^0)K^+$  events [6].

# 2 EVENT SELECTION

In this paper, measurements of the mass and width of the  $\Xi(1690)^0$  are presented. The spin of the  $\Xi(1690)^0$  is also investigated. The  $\Xi(1690)^0$  is observed in the  $\Lambda\bar{K}^0$  system produced in the decay  $\Lambda_c^+ \rightarrow (\Lambda\bar{K}^0)K^+$ , where the  $\bar{K}^0$  is reconstructed as a  $K_S \rightarrow \pi^+\pi^-$  [7]. The data sample, collected with the *BABAR* detector at the PEP-II asymmetric-energy  $e^+e^-$  collider at center-of-mass energies  $\sim 10.58$  and  $\sim 10.54$  GeV, corresponds to a total integrated luminosity of about 200 fb $^{-1}$ . The detector is described in detail elsewhere [8].

The selection of  $\Lambda_c^+$  candidates requires the intermediate reconstruction of oppositely-charged track pairs consistent with  $\Lambda \rightarrow p\pi^-$  and  $K_S \rightarrow \pi^+\pi^-$  decays. The  $\Lambda$  candidate is required to have invariant mass within a  $\pm 3\sigma$  mass window centered on its peak position, where  $\sigma$  is the mass resolution obtained from a fit to the invariant mass spectrum. The selected  $K_S$  invariant mass is within  $\pm 25$  MeV/ $c^2$  of the nominal value [1]. Each intermediate state invariant mass is then constrained to its nominal value [1], with corresponding vertex fit probability required to be greater than 0.001. The  $\Lambda$  and  $K_S$  candidates are then vertexed with a positively charged kaon track to form a  $\Lambda_c^+$  candidate. In the reconstruction, proton and kaon candidates are required to satisfy identification criteria based on specific energy loss ( $dE/dx$ ) and Cherenkov angle measurements [8]. Since the  $\Lambda$  and  $K_S$  have displaced vertices, the signal-to-background ratio is improved by requiring that each decay vertex be separated from the event primary vertex by at least of 2.5 mm in the flight direction of the  $\Lambda$  or  $K_S$ . In order to further enhance the signal-to-background ratio the center-of-mass momentum  $p^*$  of the  $\Lambda_c^+$  is required to be greater than 0.5 GeV/ $c$ .

The invariant mass spectrum of  $\Lambda_c^+$  candidates satisfying these selection criteria is shown before efficiency-correction in Fig. 1. A signal yield of  $2748 \pm 297$  candidates is obtained from a fit to the invariant mass spectrum with a double Gaussian signal function and a linear background.



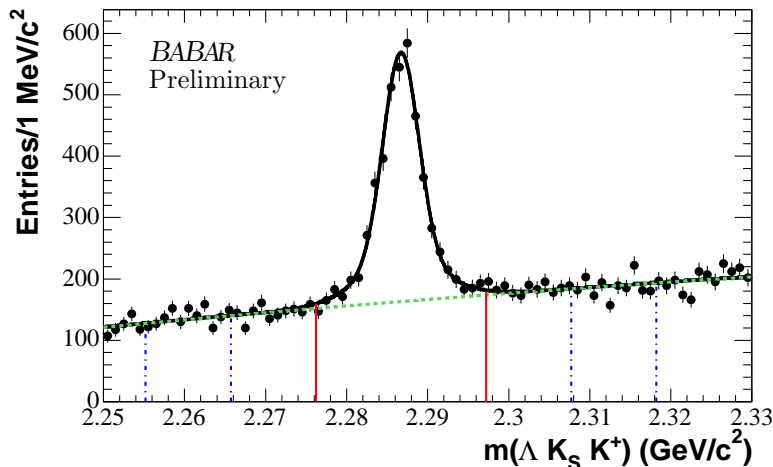


Figure 1: The invariant mass distribution of uncorrected  $\Lambda K_S K^+$  candidates in  $\sim 200 \text{ fb}^{-1}$  of data. The superimposed curve corresponds to a binned  $\chi^2$  fit which uses a double Gaussian signal function and a linear background parametrization denoted by the dashed line. The vertical lines delimit the signal region used in this analysis (solid) and the corresponding mass-sideband regions (dotted).

### 3 DALITZ PLOT FOR $\Lambda_c^+ \rightarrow \Lambda \bar{K}^0 K^+$

The Dalitz plot of  $\Lambda_c^+ \rightarrow \Lambda \bar{K}^0 K^+$  signal candidates is shown, without efficiency-correction, in Fig. 2(a). A clear band is observed in the mass-squared region of the  $\Xi(1690)^0$ , together with an accumulation of events in the  $\bar{K}^0 K^+$  threshold region. In contrast, the Dalitz plots corresponding to the  $\Lambda_c^+$  mass-sideband regions exhibit no structure. The  $\Lambda_c^+$  mass-sideband-subtracted  $\Lambda K_S$  invariant mass projection without efficiency-correction is shown in Fig. 2(b). A clear signal for the  $\Xi(1690)^0$  resonance is observed.

### 4 EFFICIENCY PARAMETRIZATION

The selection efficiency is determined from a sample of  $\Lambda_c^+ \rightarrow \Lambda \bar{K}^0 K^+$  Monte Carlo events uniformly distributed across phase-space on the Dalitz plot, and is parametrized over the entire Dalitz plot. For the measurement of the mass and width of the  $\Xi(1690)^0$ , the  $(\Lambda K_S)$  invariant mass spectrum is corrected according to an efficiency parametrized in two dimensions as a function of the cosine of the angle of the  $\Lambda$  in the  $(\Lambda K_S)$  rest-frame with respect to the  $(\Lambda K_S)$  3-momentum in the  $\Lambda_c^+$  rest-frame (i.e. the  $\Lambda$  helicity angle),  $\cos\theta_\Lambda$ , and of  $m(\Lambda K_S)$ . Each selected event is weighted inversely according to this parametrization.

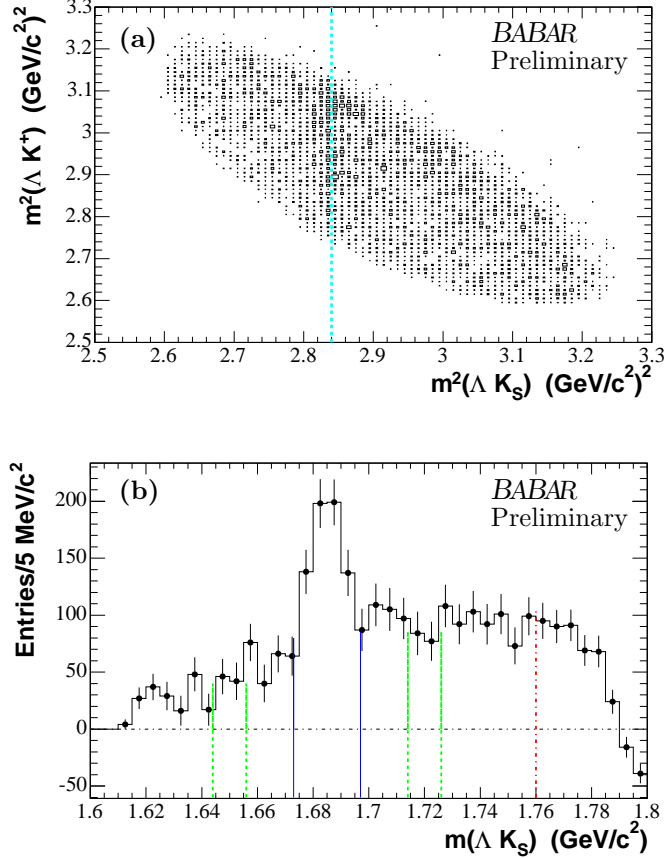


Figure 2: (a) The Dalitz plot for  $\Lambda_c^+ \rightarrow \Lambda \bar{K}^0 K^+$  corresponding to the  $\Lambda_c^+$  signal region indicated in Fig. 1. The dashed blue line indicates the nominal mass-squared region of the  $\Xi(1690)^0$ . (b) The  $\Lambda_c^+$  mass-sideband-subtracted  $\Lambda K_S$  invariant mass projection. The solid lines delimit the  $\Xi(1690)^0$  mass-signal region, while the dotted lines indicate the mass-sideband regions. The dashed line at  $1.76 \text{ GeV}/c^2$  indicates the upper limit of the uniformly accessible mass range, and corresponds to the lower bound of the  $\Lambda_c^+$  low-mass sideband.

## 5 MASS AND WIDTH MEASUREMENT

### 5.1 Resolution Smearing

For a narrow resonance such as the  $\Xi(1690)$ , the measurement of its mass and width is sensitive to detector resolution effects; in particular the apparent width will be larger than its true value. Therefore, in this measurement, the fit function is smeared by a mass resolution function, obtained from the Monte Carlo phase-space Dalitz plot in the region of the  $\Xi(1690)^0$ , and consisting of two Gaussians with a common center; a narrow Gaussian with  $\sigma = 1.07 \pm 0.02 \text{ MeV}/c^2$  and a broader Gaussian with  $\sigma = 2.44 \pm 0.06 \text{ MeV}/c^2$ . The narrow Gaussian represents 70% of the lineshape.

In order to determine the mass and width parameters of the  $\Xi(1690)^0$  resonance we parametrize its  $\Lambda_c^+$  mass-sideband-subtracted background distribution from a model of the Dalitz plot intensity distribution containing terms describing a coherent superposition of two amplitudes. The interfer-

ence between these has a significant impact on the interpretation of the apparent  $\Xi(1690)^0$  signal. The model employed and the results obtained from it are discussed in the following sub-sections.

## 5.2 Study of the $\Xi(1690)^0$ background lineshape

The accumulation of events near the  $\Xi(1690)^0$  band, towards the upper boundary of the Dalitz plot shown in Fig. 2(a), is consistent with the coherent superposition of amplitudes characterizing ( $\Lambda a_0(980)^+$ ) and ( $\Xi(1690)^0 K^+$ ) decay of the  $\Lambda_c^+$ .

The  $a_0(980)$  is known to couple to both  $\eta\pi$  and  $\bar{K}K$  and is therefore characterized by the following Flatté parametrization [9]:

$$A(a_0[980]) = \frac{g_{\bar{K}K}}{m_0^2 - m^2 - i(\rho_{\eta\pi}g_{\eta\pi}^2 + \rho_{\bar{K}K}g_{\bar{K}K}^2)}, \quad (1)$$

where  $\rho_j(m) = 2q_j/m$  is the phase space factor for the decay into the two-body channel  $j = \eta\pi, \bar{K}K$ . The coupling constants measured by the Crystal Barrel [10] and *BABAR* [11] experiments, respectively are:

$$g_{\eta\pi} = 324 \pm 15 \text{ MeV}$$

and

$$g_{\bar{K}K} = 646 \pm 29 \text{ MeV}.$$

The pole value obtained by the Crystal Barrel experiment is:

$$m_0 = 999 \pm 2 \text{ MeV}/c^2.$$

It is assumed that the  $a_0(980)^+$  is produced in an S-wave orbital angular momentum state with respect to the recoil  $\Lambda$  (although P-wave is also allowed) and that as a result no additional form factor describing the  $\Lambda_c^+$  decay to the  $\Lambda a_0(980)^+$  final state is required. It then follows that Eq. (1) describes the amplitude for this decay mode at the  $\Lambda_c^+$ , with isotropic decay of the  $a_0(980)^+$  to  $\bar{K}^0 K^+$  implied.

The angular distribution within the  $\Xi(1690)^0$  band in the Dalitz plot (Fig. 2(a)) is consistent with being flat (see section on Spin Study). Consequently, the amplitude describing the  $\Xi(1690)^0$  is chosen to be

$$A(\Xi[1690]) = \frac{1}{(m_0^2 - m^2) - im_0\Gamma(m)}, \quad (2)$$

where  $m_0 = m(\Xi(1690)^0)$ . Assuming that the  $\Lambda K_S$  system is in an S-wave state, and ignoring the contribution of other partial widths to the total width, the latter is described by

$$\Gamma(m) = \Gamma(m_0) \frac{q}{m} \frac{m_0}{q_0}, \quad (3)$$

where  $\Gamma(m_0)$  is the total width parameter to be extracted from the data, and  $q$  ( $q_0 = q(m_0)$ ) is the momentum of the  $\Lambda$  in the ( $\Lambda K_S$ ) rest-frame. As for the  $\Lambda a_0(980)^+$  amplitude, it is assumed that the  $\Xi(1690)^0$  is produced in an orbital angular momentum S-wave with respect to the recoil  $K^+$  (although P-wave is also allowed), and that no additional form factor describing  $\Lambda_c^+$  decay to  $\Xi(1690)^0 K^+$  is required. It then follows that Eq. (2) describes this decay amplitude of the  $\Lambda_c^+$  with isotropic decay to  $\Lambda \bar{K}^0$  implied.

The model is then used to describe the intensity distribution at a point on the Dalitz plot by means of the squared modulus of a coherent superposition of these two amplitudes as follows:

$$|A|^2 = |re^{i\phi}A(\Xi[1690]) + A(a_0[980])|^2, \quad (4)$$

where  $r$  represents a constant relative strength of the amplitudes and  $\phi$  is a constant relative phase between them.

In order to test the model and obtain appropriate values for  $r$  and  $\phi$ , a width  $\Gamma(m_0) = 10$  MeV is assumed for the  $\Xi(1690)^0$  in the expression for  $A(\Xi[1690])$ . The corresponding values for  $r$ , and  $\phi$  are then obtained from a simultaneous  $\chi^2$  minimization between the simulated  $\Lambda K_S$ ,  $K_S K^+$  and  $\Lambda K^+$  invariant mass spectra and the corresponding projections in data. The minimum  $\chi^2$  corresponds to  $\phi = 34$  deg. and  $r = 0.025$ . In Fig. 3, the  $m(\Lambda K_S)$ ,  $m(K_S K^+)$  and  $m(\Lambda K^+)$  Monte Carlo projections weighted by the resulting  $|A|^2$  are represented by the histograms superimposed on the open circles corresponding to the efficiency-corrected distributions in data, and it is clear that the simple model describes the mass projections very well. The green and blue points correspond to the Monte Carlo projections weighted by the terms  $|A(a_0[980])|^2$  and  $|A|^2 - r^2|A(\Xi[1690])|^2$ , respectively, where the latter represents the resulting total background in the  $(\Lambda K_S)$  mass distribution (after  $\Lambda_c^+$  mass-sideband-subtraction). The main feature of this background is the presence of a peak in the  $\Xi(1690)^0$  signal region that results from the interference between the  $\Xi(1690)^0$  and the  $a_0(980)^+$  amplitudes.

### 5.3 Measurement Procedure

Previous measurements of the mass and width of the  $\Xi(1690)$  resonance relied on a fit to the signal making an ad hoc polynomial assumption about the shape of an incoherent background [6]. Based on the agreement between the weighted Dalitz plot projections obtained from simulation and the data of Fig. 3, it is apparent that a background description of the  $m(\Lambda \bar{K}^0)$  spectrum based on a polynomial parametrization does not take adequate account of the physics process involved in the description of the Dalitz plot.

The procedure adopted to fit the sideband-subtracted, efficiency-corrected  $(\Lambda K_S)$  invariant mass distribution shown by the open circles of Fig. 4 is therefore as follows:

(i) The mass distribution is parametrized by means of the function

$$f = c_1 \frac{pq}{M} |A(1690)|^2 + c_2 \left[ |A(980)|^2 + 2\text{Re}(re^{-i\phi} A(1690)^* A(980)) \right]. \quad (5)$$

The first term represents the lineshape of the  $\Xi(1690)^0$ , and incorporates the resolution smearing procedure discussed previously. The second term is the total background due to the  $a_0(980)^+$  and its interference with the  $\Xi(1690)^0$ ;  $M$  is the  $\Lambda_c^+$  mass,  $p$  is the momentum of the  $K^+$  in the  $\Lambda_c^+$  rest-frame, and  $q$  is the momentum of the  $\Lambda$  in the  $(\Lambda K_S)$  rest-frame. The lineshape for the latter term is obtained by simulation, incorporating fixed values for  $\phi$ ,  $m_0$ , and  $\Gamma(m_0)$ , obtained by the iteration described below. The first term corresponds to the actual fit function where  $m_0$  and  $\Gamma(m_0)$  are parameters.

(ii) In the second term, the phase  $\phi$  is fixed at values which are varied in one degree steps from 15 deg – 50 deg. The value for  $r$  is obtained by the simultaneous minimization of the  $\chi^2$  of the mass projections of Fig. 3.

(iii) The fit procedure for each choice of  $\phi$  is iterative, in that the values of  $r$ ,  $m_0$  and  $\Gamma(m_0)$  used in the second term are fixed to those from the previous iteration, and the value of  $\Gamma(m_0)$

also incorporates the effect of resolution smearing; the  $(\Lambda K_S)$  mass projection due to this term is

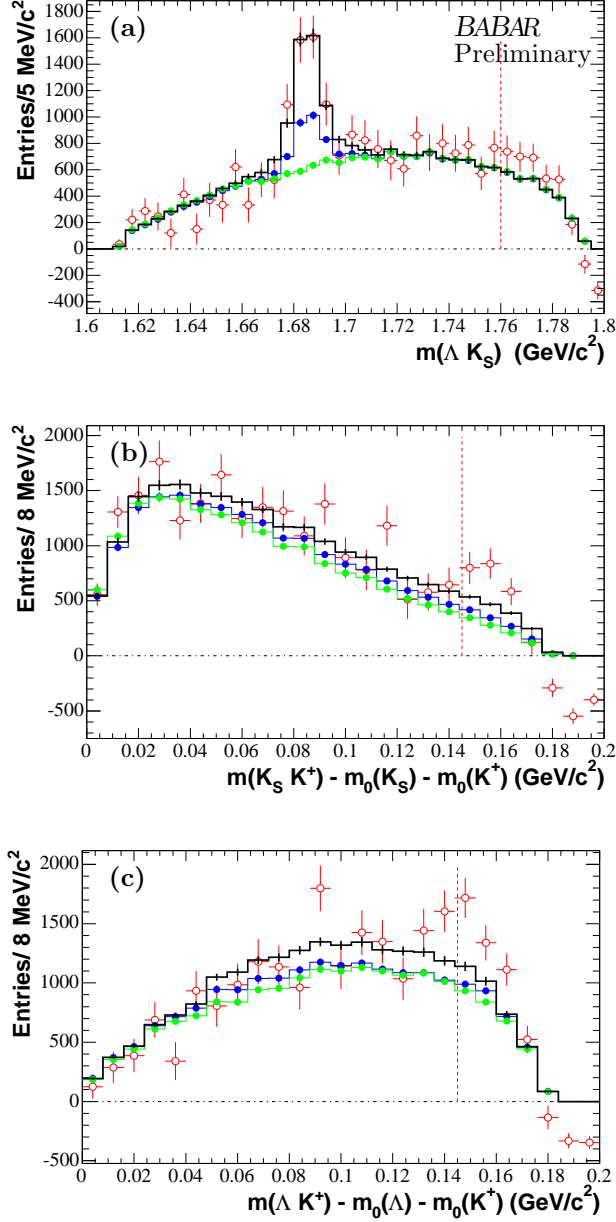


Figure 3: The  $m(\Lambda K_S)$  (a),  $(K_S K^+)$  mass difference with respect to threshold (b), and  $(\Lambda K^+)$  mass difference with respect to threshold (c) Monte Carlo projections weighted by  $|A|^2$  are shown as the histograms superimposed on the open circles corresponding to the efficiency-corrected distributions in data. The light-colored (green) and dark-colored (blue) points correspond to the Monte Carlo projections weighted by the terms  $|A(a_0[980])|^2$  and  $|A|^2 - r^2|A(\Xi[1690])|^2$ , respectively, where these model parameters are given in Eq. 4. As in Fig. 2(b), the vertical dashed lines indicate the upper limit of the uniformly accessible mass range.

obtained by weighting the MC phase space distribution.

(iv) The procedure converges typically after two iterations in the sense that  $m_0$  and  $\Gamma(m_0)$  no longer change.

The width value of 10 MeV shown in Fig. 3 corresponds to the initial value of the iteration process. The results of the best fit obtained by this procedure are shown in Fig. 4 in comparison to the background-subtracted, efficiency-corrected ( $\Lambda K_S$ ) mass distribution (open circles with error bars).

The value  $\Gamma(m_0) = 9.5$  MeV with  $m_0 = 1684.7$  MeV/ $c^2$  used in the second term of Eq. (5) was obtained by the iteration procedure, starting at  $\Gamma(m_0) = 10$  MeV with  $m_0 = 1685.0$  MeV/ $c^2$ . The histogram represents the total contribution in each mass interval obtained from the fit.

The value for the total  $\Xi(1690)^0$  signal yield obtained from this fit is  $1837 \pm 463$  events. The peaking background due to the interference with the  $a_0(980)^+$  results in a signal yield about 30% smaller than would be obtained with a fit using an incoherent polynomial background.

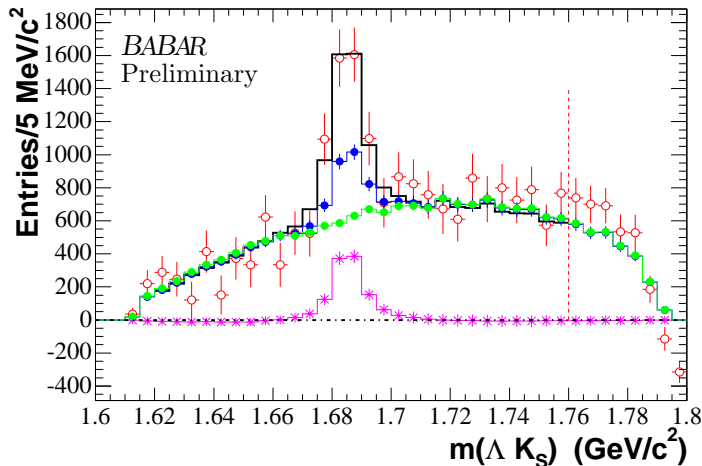


Figure 4: The ( $\Lambda K_S$ ) invariant mass projection in data, after all corrections, is represented by the open circles. Superimposed is the distribution for the simulated interference term  $2\text{Re}(re^{-i\phi}A(1690)^*A(980))$  (represented by the stars), the  $|A(980)|^2$  distribution (light-colored dots), and (dark-colored dots) the total background obtained as the sum of these contributions. The value  $\Gamma(m_0) = 9.5$  MeV, after resolution smearing, (obtained by iteration), and  $\phi = 34$  deg. have been used in obtaining the background distribution. The histogram represents the total contribution in each mass interval, and is obtained from the fit as the sum of the  $\Xi(1690)^0$  signal smeared by resolution and the total background contribution. This fit has a  $\chi^2/NDF$  of 20/24.

## 5.4 Systematic Uncertainties

The dominant sources of systematic uncertainty in this measurement are due to the choice of phase,  $\phi$ , entering the  $\Xi(1690)^0$  background distribution through the second term in Eq. (5). From the fits described above for different choices of phase value, it is found that the values yielding a  $\chi^2$  increase of one unit relative to the minimum are  $\phi = 21$  deg and  $\phi = 46$  deg, respectively. The shape of the interference term between the  $a_0(980)^+$  and the  $\Xi(1690)^0$  amplitudes has a tail to high mass and a sharp rise at low mass for  $\phi = 21$  deg and vice-versa for  $\phi = 46$  deg. This effect causes the fitted  $\Xi(1690)^0$  mass value to shift significantly, and this must be taken into account as a systematic uncertainty. The corresponding effect on the width proves to be quite small.

A second source of systematic uncertainty results from the choice of  $\Lambda_c^+$  mass sidebands. Up to this point, the  $\Lambda_c^+$  mass sidebands used for the  $\Xi(1690)^0$  mass and width measurement as well as for the study of systematic uncertainties corresponded to  $\pm 6\sigma$  to  $\pm 9\sigma$  from the  $\Lambda_c^+$  fitted mean. The entire fit procedure is repeated first using  $\Lambda_c^+$  mass sidebands which are from  $\pm 7.5\sigma$  to  $\pm 10.5\sigma$  from the  $\Lambda_c^+$  fitted mean, and then  $\Lambda_c^+$  mass sidebands which are from  $\pm 4.5\sigma$  to  $\pm 7.5\sigma$  from the  $\Lambda_c^+$  fitted peak value. The associated systematic uncertainties in mass and width are then estimated as one half of the difference in the fit values obtained.

The effect of the efficiency parametrization on the fit results is found to be negligible.

In the definition of the  $\Xi(1690)^0$  amplitude used in the fits it has been assumed that the orbital angular momentum in  $\Lambda_c^+$  decay is  $L = 0$  and that the orbital angular momentum in the decay of the  $\Xi(1690)^0$  to  $\Lambda\bar{K}^0$  system is  $l = 0$ . The fit procedure is repeated using  $L = 0$  and  $l = 1$ ,  $L = 1$  and  $l = 1$ , and  $L = 1$  and  $l = 0$ . The effect on fitted mass and width is small, and corresponding systematic uncertainties are estimated as the extrema of the changes which result.

Effects due to the uncertainties in the respective widths of the narrow and wide Gaussians used to parametrize the lineshape of the resolution function are also considered. The fitting procedure is repeated incorporating resolution smearing, with the values of the Gaussian widths shifted by  $\pm 1$  standard deviation, and the resulting mass and width changes are found to be small.

The width of the  $\Lambda_c^+$  signal in data and MC agree to better than 10%. The width of the resolution function used in smearing the  $\Xi(1690)^0$  lineshape is therefore increased by 10%, and the fitted value of the  $\Xi(1690)^0$  width is found to decrease by 0.2 MeV. This effect is also included in the estimate of systematic uncertainty associated with resolution.

Uncertainties due to detector effects are estimated from the study of systematic uncertainties in the mass measurement of the  $\Lambda_c^+$  using  $\Lambda_c^+ \rightarrow \Lambda K_S K^+$  and  $\Lambda_c^+ \rightarrow \Sigma K_S K^+$  decays [12]. This study found that the dominant systematic uncertainty in mass arose from the amount of material in the tracking volume and from the magnetic field strength, but that this effect was small for  $\Lambda_c^+ \rightarrow \Lambda\bar{K}^0 K^+$  because of the limited phase space available in the decay. Because systematic uncertainties scale with Q-value, we obtain a conservative estimate of the uncertainty due to detector effects in the decay  $\Lambda_c^+ \rightarrow \Xi(1690)^0 K^+$  based the uncertainty determined from  $\Lambda_c^+ \rightarrow \Lambda\bar{K}^0 K^+$ . Thus, we quote a systematic uncertainty of  $\pm 0.1$  MeV/ $c^2$  on the  $\Xi(1690)^0$  mass.

Table 1 summarizes the systematic uncertainties associated with the mass and width measurements of the  $\Xi(1690)^0$ .

Source of Syst. Error	Mass Error	Width Error
choice of relative phase	$^{+2.1}_{-1.5}$ MeV/ $c^2$	+0.3 MeV
choice of $A_c^+$ mass sidebands	$\pm 0.4$ MeV/ $c^2$	$\pm 0.8$ MeV
efficiency parametrization	$\pm 0.1$ MeV/ $c^2$	$\pm 0.3$ MeV
choice of $L, l$	$\pm 0.2$ MeV/ $c^2$	$\pm 0.3$ MeV
resolution function lineshape	$-0.1$ MeV/ $c^2$	$^{+0.1}_{-0.2}$ MeV
detector effects	$\pm 0.1$ MeV/ $c^2$	0.0 MeV
Total Systematic Error	$^{+2.2}_{-1.6}$ MeV/ $c^2$	$^{+1.0}_{-0.9}$ MeV

Table 1: Summary of systematic uncertainties associated with the measurements of the mass and width of the  $\Xi(1690)^0$ .

## 5.5 Summary of Results

The measured values of the mass and width of the  $\Xi(1690)^0$  obtained in the present analysis are as follows:

$$m(\Xi(1690)) = 1684.7 \pm 1.3 \text{ (stat.) } ^{+2.2}_{-1.6} \text{ (syst.) MeV}/c^2,$$

$$\Gamma(\Xi(1690)) = 8.1 ^{+3.9}_{-3.5} \text{ (stat.) } ^{+1.0}_{-0.9} \text{ (syst.) MeV}.$$

The uncertainty in the mass value is mainly systematic, and results primarily from the interference between the  $\Xi(1690)^0$  and  $a_0(980)^+$  amplitudes. In contrast, the width uncertainty is primarily statistical in nature.

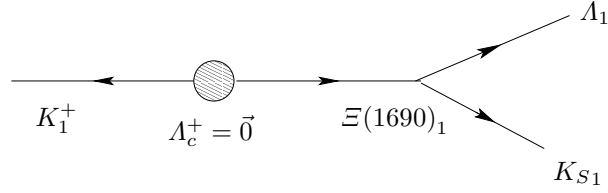
## 6 SPIN STUDY

For the decay of a spin 1/2 charm baryon to a hyperon and a pseudo-scalar meson (where the former decays to a secondary hyperon and a pseudo-scalar meson), the angular distribution of the decay products can be determined unambiguously, by choosing the quantization axis along the direction of the primary hyperon in the charm baryon rest-frame, such that the helicity  $\lambda_i$  of the primary hyperon can only take the values  $\pm 1/2$ . The probability for the secondary hyperon to emerge with Euler angles  $(\phi, \theta, 0)$  with respect to the quantization axis, is given by the square of the amplitude characterizing the decay of a primary hyperon (in this case the  $\Xi(1690)^0$  resonance) with total angular momentum  $J$  and helicity  $\lambda_i$  to a 2-body system with net helicity  $\lambda_f$ :

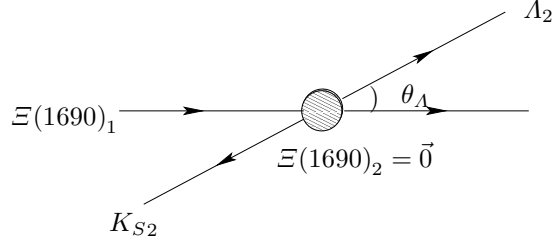
$$A_{\lambda_f}^J D_{\lambda_i \lambda_f}^{J*}(\phi, \theta, 0),$$

where the transition matrix element  $A_{\lambda_f}^J$  represents the coupling of the  $\Xi(1690)^0$  to the final state;  $A_{\lambda_f}^J$  does not depend on  $\lambda_i$  because of rotational invariance [13, 14, 15, 16]. The helicity angle  $\theta$ , illustrated in Fig. 5, is defined as the angle between the direction of the secondary hyperon in the primary hyperon rest-frame and the direction of the primary hyperon in the charm baryon





a) All decay products in the  $\Lambda_c^+$  rest-frame.



b) All decay products in the  $\Xi(1690)^0$  rest-frame;  
in this frame,  $\Xi(1690)_1 \rightarrow \Xi(1690)_2 = \vec{0}$ ,  
 $\Lambda_1 \rightarrow \Lambda_2$ ,  $K_{S1} \rightarrow K_{S2}$ .

Figure 5: Schematic definition of the helicity angle  $\theta_\Lambda$  in the decay chain  $\Lambda_c^+ \rightarrow \Xi(1690)^0 K^+$ ,  $\Xi(1690)^0 \rightarrow \Lambda K_S$ ; as shown in b)  $\theta_\Lambda$  is the angle between the  $\Lambda$  direction in the  $\Xi(1690)^0$  rest-frame and the  $\Xi(1690)^0$  direction in the  $\Lambda_c^+$  rest-frame.

rest-frame. The angular distribution of the secondary hyperon is then given by the total intensity,

$$I \propto \sum_{\lambda_i, \lambda_f} \rho_i \left| A_{\lambda_f}^J D_{\lambda_i \lambda_f}^{J*}(\phi, \theta, 0) \right|^2$$

where  $\rho_i$  ( $i = \pm 1/2$ ) are the diagonal density matrix elements inherited from the charm baryon, and the sum is over all initial and final helicity states. Previous studies [17] have indicated that in an inclusive environment the parent baryon diagonal density matrix elements are equally populated. Thus, the helicity angular distribution contains no dependence on the  $\Lambda_c^+$  density matrix elements. Using the above expression, the angular distribution of the  $\Lambda$  decay product of the  $\Xi(1690)^0$  is computed according to different spin hypotheses for the  $\Xi(1690)^0$ :

$$J_{\Xi(1690)} = 1/2 \quad : \quad 1 \tag{6}$$

$$J_{\Xi(1690)} = 3/2 \quad : \quad \frac{1}{4}(1 + 3\cos^2\theta_\Lambda) \tag{7}$$

$$J_{\Xi(1690)} = 5/2 \quad : \quad \frac{1}{4}(1 - 2\cos^2\theta_\Lambda + 5\cos^4\theta_\Lambda) \tag{8}$$

The above equations ignore the presence of a coherent amplitude describing the  $K_S K^+$  structure in the  $\Lambda_c^+$  Dalitz plot. As discussed above, there is evidence of such structure. Nevertheless, the decay angular distribution of the  $\Xi(1690)^0$  is investigated by means of a sideband subtraction procedure and the MC model of the Dalitz plot structure is used to take account of systematic effects due to  $a_0(980)^+$  interference.

The  $\Xi(1690)^0$  mass-sideband-subtracted  $\cos\theta_\Lambda$  distribution in data is shown in Fig. 6. The distribution has been corrected with an efficiency calculated for each  $\cos\theta_\Lambda$  interval from phase space  $\Lambda_c^+ \rightarrow \Lambda \bar{K}^0 K^+$  Monte Carlo. The horizontal line represents the expected distribution for

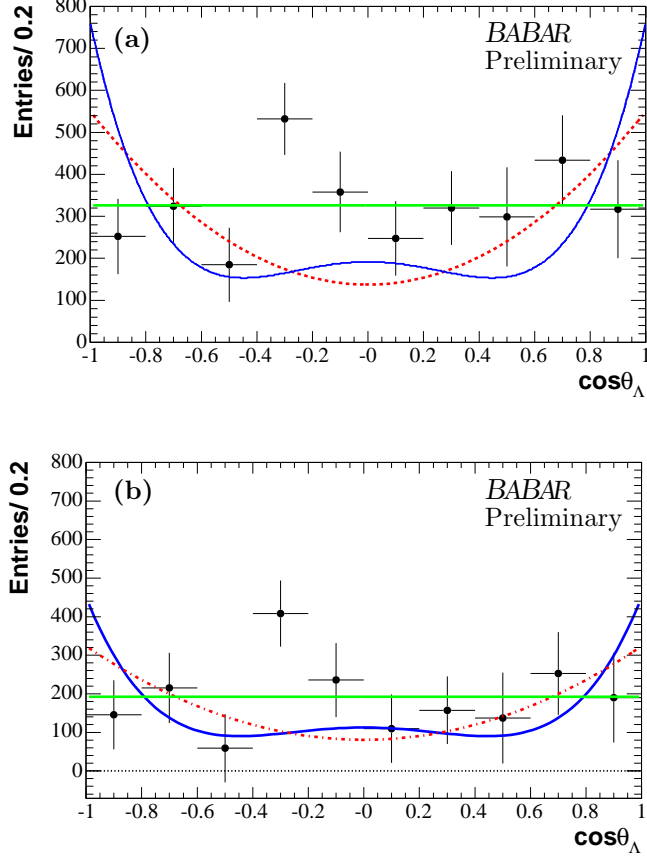


Figure 6: The  $\Lambda_c^+$  mass-sideband-subtracted,  $\Xi(1690)^0$  mass-sideband-subtracted, efficiency-corrected  $\cos\theta_\Lambda$  distribution in data. The horizontal line represents the expected distribution for  $J_{\Xi(1690)} = 1/2$ , the dashed curve corresponds to  $J_{\Xi(1690)} = 3/2$ , while the solid curve corresponds to  $J_{\Xi(1690)} = 5/2$ . In Fig. (a) no correction has been made for Dalitz plot interference effects. Fig (b) shows the resulting distribution after correction for Dalitz plot interference effects.

$J_{\Xi(1690)}$	Fit $\chi^2/\text{NDF}$	Fit C.L.	Comment
1/2	11.0/9	0.28	Fig. 6(a), solid line
3/2	35.7/9	$4 \times 10^{-5}$	Fig. 6(a), dashed curve
5/2	42.9/9	$2 \times 10^{-6}$	Fig. 6(a), solid curve

Table 2: The  $\cos\theta_\Lambda$  angular distribution fit C.L. values of Fig. 6(a) corresponding to  $\Xi(1690)^0$  spin hypotheses 1/2, 3/2 and 5/2 for  $\Xi(1690)^0 \rightarrow \Lambda\bar{K}^0$  data assuming  $J_{\Lambda_c} = 1/2$ . No correction has been made for Dalitz plot interference effects.

$J_{\Xi(1690)} = 1/2$ , the dashed curve corresponds to  $J_{\Xi(1690)} = 3/2$ , while the solid curve corresponds to  $J_{\Xi(1690)} = 5/2$  (Eqs. (6) - (8), respectively). The fit C.L. values are summarized in Table 2.

In Fig. 7 the results of treating the MC model of the Dalitz plot intensity distribution in the same way are shown (where the parameters of the MC model are the ones of Fig. 4). As the Monte

$J_{\Xi(1690)}$	Fit $\chi^2/\text{NDF}$	Fit C.L.	Comment
1/2	10.8/9	0.30	Fig. 6(b), solid line
3/2	19.5/9	0.02	Fig. 6(b), dashed curve
5/2	21.7/9	0.01	Fig. 6(b), solid curve

Table 3: The  $\cos\theta_\Lambda$  angular distribution fit C.L. values of Fig. 6(b) corresponding to  $\Xi(1690)^0$  spin hypotheses 1/2, 3/2 and 5/2 for  $\Xi(1690)^0 \rightarrow \Lambda\bar{K}^0$  data assuming  $J_{\Lambda_c} = 1/2$ , after correction for Dalitz plot interference effects.

Carlo sample used contains no spin angular structure, it is equivalent to the generation of events with the  $(\Lambda\bar{K}^0)$  system in a spin 1/2 (S-wave) state. In Fig. 7(a) the upper points correspond to the simulated data points of Fig. 6(a), while the solid points result from the contribution to the Dalitz plot intensity from the  $a_0(980)^+$  and its interference with the  $\Xi(1690)^0$ . Both distributions rise slightly towards  $\cos\theta_\Lambda = 1$ . However, the difference between them, shown in Fig. 7(b), is quite flat as indicated by the dashed line. The distribution in Fig. 7(a) represented by the solid points is used to correct the data points of Fig. 6(a) to give the distribution of Fig. 6(b), and the new fit results for the different assumptions about the  $\Xi(1690)^0$  spin are summarized in Table 3. The spin 1/2 hypothesis is favored, but not as strongly as would be inferred from Table 2. This reduced discrimination is due primarily to the fact that the background distribution due to  $a_0(980)^+$  and its interference with the  $\Xi(1690)^0$  (represented by the solid points in Fig. 7(a)) accounts for  $\sim 30\%$  of the apparent signal in the  $\Xi(1690)^0$  region, as shown in Fig. 4, and it is this reduction in  $\Xi(1690)^0$  signal size which affects the C.L. values for the spin 3/2 and 5/2 hypotheses.

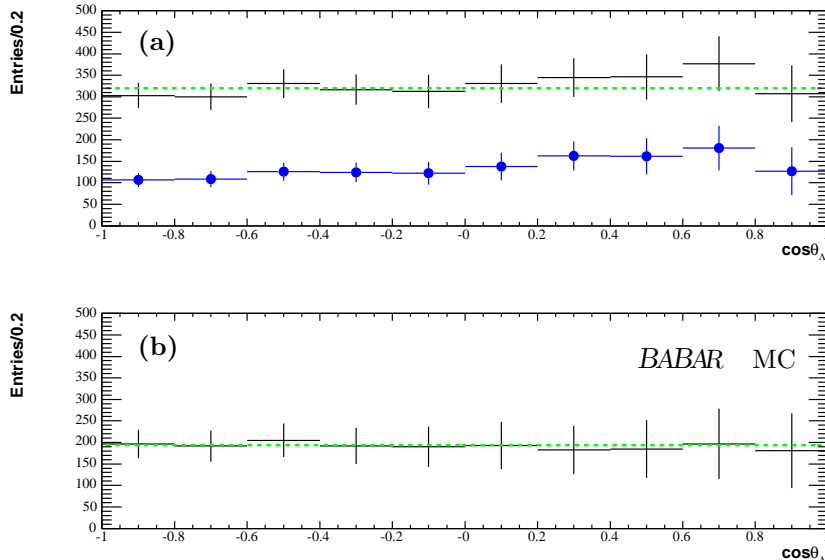


Figure 7: The MC efficiency-corrected  $\Xi(1690)^0$  mass-sideband-subtracted  $\cos\theta_\Lambda$  distribution obtained from the  $a_0(980)^+-\Xi(1690)^0$  Dalitz plot model. In Fig. 7(a) the vertical crosses result from the same sideband subtraction procedure applied to data, while the contribution from the  $\Xi(1690)^0$  background is represented by the solid points. In Fig. 7(b) the  $\cos\theta_\Lambda$  distribution for the  $\Xi(1690)^0$  only is obtained after subtraction of the distributions shown in Fig. 7(a). The rise at high  $\cos\theta_\Lambda$  seen in Fig. 7(a) is due to interference effects in the Dalitz plot. The subtraction procedure makes the distribution shown in Fig. 7(b) flat, as expected.

## 7 CONCLUSIONS

An analysis of the amplitude structure in the  $\Lambda_c^+ \rightarrow \Lambda K_S K^+$  Dalitz plot has resulted in the following values for the mass and width of the  $\Xi(1690)^0$ :

$$m(\Xi(1690)) = 1684.7 \pm 1.3 \text{ (stat.) } {}_{-1.6}^{+2.2} \text{ (syst.) MeV}/c^2,$$

$$\Gamma(\Xi(1690)) = 8.1 {}_{-3.5}^{+3.9} \text{ (stat.) } {}_{-0.9}^{+1.0} \text{ (syst.) MeV.}$$

The spin of the  $\Xi(1690)$  is consistent with 1/2, from fits to the angular distribution in data and MC.

We are grateful for the extraordinary contributions of our PEP-II colleagues in achieving the excellent luminosity and machine conditions that have made this work possible. The success of this project also relies critically on the expertise and dedication of the computing organizations that support *BABAR*. The collaborating institutions wish to thank SLAC for its support and the kind hospitality extended to them. This work is supported by the US Department of Energy and National Science Foundation, the Natural Sciences and Engineering Research Council (Canada), Institute of High Energy Physics (China), the Commissariat à l’Energie Atomique and Institut National de Physique Nucléaire et de Physique des Particules (France), the Bundesministerium für

Bildung und Forschung and Deutsche Forschungsgemeinschaft (Germany), the Istituto Nazionale di Fisica Nucleare (Italy), the Foundation for Fundamental Research on Matter (The Netherlands), the Research Council of Norway, the Ministry of Science and Technology of the Russian Federation, and the Particle Physics and Astronomy Research Council (United Kingdom). Individuals have received support from the Marie-Curie IEF program (European Union) and the A. P. Sloan Foundation.

## References

- [1] Particle Data Group, S. Eidelman *et al.*, Phys. Lett. **B592**, 1 (2004).
- [2] C. Dionisi *et al.*, Phys. Lett. **B80**, 145 (1978).
- [3] S.F. Biagi *et al.*, Z. Phys. C **9**, 305 (1981).
- [4] S.F. Biagi *et al.*, Z. Phys. C **34**, 15 (1987).
- [5] M.I. Adamovich *et al.*, Eur. Phys. J. **C5**, 621 (1998).
- [6] K. Abe *et al.*, Phys. Lett. **B524**, 33 (2002).
- [7] Charge conjugation is implied throughout this paper.
- [8] B. Aubert *et al.*, Nucl. Instrum. Methods A **479**, 1 (2002).
- [9] S. M. Flatté, Phys. Lett. **B63**, 224 (1976).
- [10] A. Abele *et al.*, Phys. Rev. **D57**, 3860 (1998).
- [11] B. Aubert *et al.*, Phys. Rev. **D72**, 052008 (2005).
- [12] B. Aubert *et al.*, Phys. Rev. **D72**, 052006 (2005).
- [13] M. Jacob and G. C. Wick, Ann. Phys. **7**, 404 (1959).
- [14] S. U. Chung, CERN Yellow Report, CERN 71-8 (1971).
- [15] E. Wigner, Z. Phys. **43**, 624 (1927);  
C. Eckart, Rev. Mod. Phys. **2**, 305 (1930).
- [16] H. L. Anderson, E. Fermi, E. A. Land and D. E. Nagle, Phys. Rev. **85**, 936 (1952).
- [17] B. Aubert *et al.*, hep-ex/0606039.